Journal of Alloys and Compounds 704 (2017) 206–211

Contents lists available at ScienceDirect

Journal of Alloys and Compounds

journal homepage: http://www.elsevier.com/locate/jalcom

The dominant role of excitation diffusion in energy transfer upconversion of Lu_2O_3: Tm^{3+}, Yb^{3+}

Dan Wu [a, b], Zhendong Hao [a, *], Wenge Xiao [a, b], Xia Zhang [a], Guo-Hui Pan [a], Liangliang Zhang [a], Yongshi Luo [a], Ligong Zhang [a], Haifeng Zhao [a], Jiahua Zhang [a, **]

[a] State Key Laboratory of Luminescence and Applications, Changchun Institute of Optics, Fine Mechanics and Physics, Chinese Academy of Sciences, Changchun, 130033, Jilin, China
[b] University of Chinese Academy of Sciences, Beijing, 100049, China

ARTICLE INFO

Article history:
Received 31 October 2016
Received in revised form
29 January 2017
Accepted 30 January 2017
Available online 2 February 2017

Keywords:
Upconverted NIR emission
Tm^{3+}-Yb^{3+}
Excitation diffusion

ABSTRACT

Emission spectra of Tm^{3+} and Yb^{3+} codoped Lu_2O_3 are studied as a function of the dopant concentration upon 980 nm excitation. The upconverted near infrared emission around 811 nm from Tm^{3+}:$^3H_4 \rightarrow {}^3H_6$ transition is observed due to two step energy transfers from Yb^{3+} through Tm^{3+}:$^3F_4$ as the intermediate level. The optimal dopants concentrations for the strongest upconversion emission are 0.1 mol% Tm^{3+} and 4 mol% Yb^{3+}. The dependence of energy transfer coefficients for the two step energy transfers on Tm^{3+} and/or Yb^{3+} concentration is studied. The obtained results indicate that the excitation diffusions among Yb^{3+} ions and among Tm^{3+} ions mainly control the energy transfer rates for the optimal dopants concentrations and thus dominate the energy transfer upconversion process.

1. Introduction

Recently, Rare earth (RE) ions doped near infrared (NIR) to NIR upconversion luminescence (UCL) materials have drawn considerable attention for their potential applications in optical bioimaging in the NIR window (650–1000 nm) for biological tissues [1–7]. As with Er^{3+}, Ho^{3+}, Nd^{3+} ions, Tm^{3+} ion is widely used as an activator because of its complicate energy levels allowing the emission band vary from ultraviolet to infrared [8]. The combination of Tm^{3+} and Yb^{3+} forms one of the most attractive energy transfer upconversion (ETU) system [9–12]. In this system, Yb^{3+} acts as an efficient sensitizer upon NIR (980 nm) excitation due to its large absorption cross section [13,14] and Tm^{3+}:$^3H_4$ level can be populated by two steps energy transfer from Yb^{3+} and then generates intense shorter wavelength NIR emission at 811 nm originating from $^3H_4 \rightarrow {}^3H_6$ transition, which matches well with the bio-optical window. The Tm^{3+} and Yb^{3+} codoped materials have been considered as one of the typical donor-acceptor systems for upconversion and infrared materials [15,16].

Oxide materials usually have stable chemical and thermal properties and could be promising hosts for UCL [17–19]. As one of the rare earth sesquioxides, there have been some reports focusing on UV and NIR upconversion emissions in the range of 400–850 nm in Tm^{3+} and Yb^{3+} codoped Lu_2O_3, but the role of excitation diffusion in energy transfer process was rarely studied [20,21]. Since the donors and acceptors are randomly distributed in space, the distance between a donor and an acceptor also has a distribution. The direct energy transfer from a donor to a distant acceptor is ineffective, but the excitation energy of the donor can be efficiently transferred to the acceptor through excitation diffusion to another donor in the vicinity of the acceptor [22]. As a result, the excitation diffusion in heavily doped systems is notable, such as in heavily Yb^{3+} doped ETU materials. In Tm^{3+}-Yb^{3+} ETU system the upconverted NIR emission is performed by two step energy transfers, i.e. the first step excitation from Tm^{3+}:$^3H_6$ to $^3F_4$ level and the second step excitation from Tm^{3+}:$^3F_4$ to $^3H_4$ level. It has been observed that each of the excitations by energy transfer is efficient even for low Tm^{3+} doping in some materials [23–25]. This means that the excitation diffusion may play an important role in promoting the energy transfer process.

In the present work, we have studied the downconversion and upconversion luminescence properties simultaneously in the range from 700 to 1700 nm upon 980 nm excitation as a function of Tm^{3+} or Yb^{3+} concentration in Lu_2O_3. Although researchers have carried out extensive studies on UV and NIR upconversion emissions in

* Corresponding author.
** Corresponding author.
E-mail addresses: haozd@ciomp.ac.cn (Z. Hao), zhangjh@ciomp.ac.cn (J. Zhang).

http://dx.doi.org/10.1016/j.jallcom.2017.01.344
0925-8388/

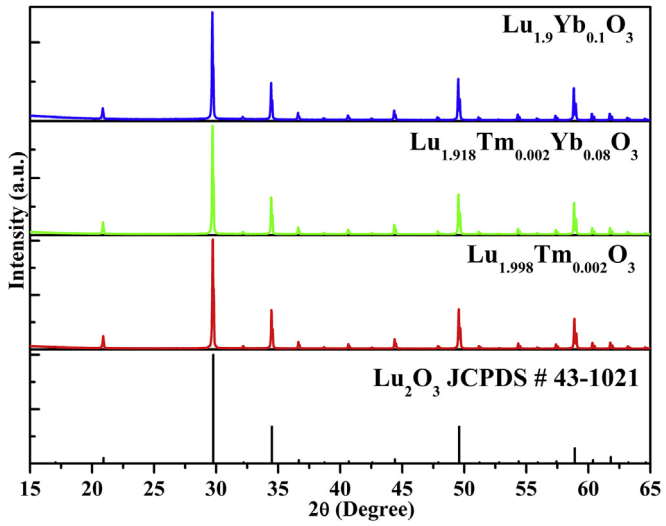

Fig. 1. XRD patterns of Tm^{3+}, Yb^{3+} singly and doubly doped Lu_2O_3, the standard pattern of Lu_2O_3 (JCPDS 43–1021) is also presented for comparison.

Tm^{3+} and Yb^{3+} codoped materials, it should be mentioned that few of them pay attention to the downconversion emissions [26,27]. Since the first step dominates the upconversion process, the study of the Tm^{3+}:$^3F_4$ level is necessary for understanding the upconversion process. In our work, the strongest upconverted NIR emission from Tm^{3+}:$^3H_4 \rightarrow {}^3H_6$ transition around 811 nm appears at 0.1 mol% Tm^{3+} and 4 mol% Yb^{3+}. The dependence of the emission intensities of Tm^{3+}:$^3F_4$, $^3H_4$ levels and Yb^{3+}:$^2F_{5/2}$ level on Tm^{3+} and/or Yb^{3+} concentration is analyzed. Steady state equation model is adopted to understand the influence of excitation diffusion on the energy transfer rate in the two step energy transfers. The obtained results indicate that the excitation diffusions among Yb^{3+} ions and among Tm^{3+} ions substantially enhance the rate of energy transfer from Yb^{3+} to Tm^{3+} and thus dominate the ETU process.

2. Experimental

2.1. Sample preparation

Three series of samples $Lu_{2(0.95-x)}Tm_{2x}Yb_{0.1}O_3$ ($x = 0.0005–0.01$), $Lu_{2(0.999-y)}Tm_{0.002}Yb_{2y}O_3$ ($y = 0–0.1$) and $Lu_{2(1-y)}Yb_{2y}O_3$ ($y = 0.005–0.1$) were synthesized via the normal firing precursor method. The firing precursor is considered to be more favorable to obtain uniform and highly crystallized samples than the traditional solid-state reaction. The appropriate amounts of Lu_2O_3 (5N), Tm_2O_3 (5N) and Yb_2O_3 (6N) were first dissolved in dilute nitric acid (G.R.), to get the $Lu(NO_3)_3$, $Tm(NO_3)_3$ and $Yb(NO_3)_3$ solutions, respectively. $Tm(NO_3)_3$, and $Yb(NO_3)_3$ solutions with corresponding moles ratio were added into $Lu(NO_3)_3$ solution, and the mixed solution was stirred vigorously at room temperature to form a homogeneous solution. The resulting solution was dried at 95 °C for 24 h and then preheated at 700 °C for 3 h to remove the nitrate (NO_3^-). After grinding, the precursor was put into an alumina crucible and sintered at 1600°C for 5 h in air.

2.2. Measurements and characterization

The crystal structure of samples were characterized by X-ray diffraction (XRD) (Rigaku D/max-rA power diffractometer using Cu Kα ($\lambda = 1.54178$ Å) radiation). The emission spectra were measured using FLS920 spectrometer (Edinburgh Instruments, U.K.). In fluorescence lifetime measurements, an optical parametric oscillator (OPO) was used as an excitation source and the signal was detected by a Tektronix digital oscilloscope (TDS 3052). All the measurements were obtained at room temperature.

3. Results and discussion

The XRD patterns of the three representative Tm^{3+} and/or Yb^{3+} doped Lu_2O_3 samples are shown in Fig. 1. It is obvious that all the diffraction peaks of the samples can be well indexed to the cubic structure of Lu_2O_3 (JCPDS NO. 43–1021) and no detectable impurities are presented, indicating the formation of Lu_2O_3 pure phase.

The emission intensities as a function of Tm^{3+} and/or Yb^{3+} concentration are studied upon 980 nm excitation. Fig. 2a shows the emission spectra for a fixed Yb^{3+} concentration at 5 mol% and various Tm^{3+} concentrations (0.05–1 mol%) in Lu_2O_3 upon 980 nm diode laser excitation with a low output power density of 7 mW/mm^2. The upconverted NIR emission appears at 811 nm, originating from Tm^{3+}:$^3H_4 \rightarrow {}^3H_6$ transition. The typical Yb^{3+}: $^2F_{5/2} \rightarrow {}^2F_{7/2}$ emission in the range of 1000 nm–1200 nm and Tm^{3+}: $^3F_4 \rightarrow {}^3H_6$ emission around 1630 nm are also observed. It is noted that only a part of Tm^{3+}: $^3F_4 \rightarrow {}^3H_6$ emission is detected around 1630 nm because the In GaAs detector used has a cutoff wavelength of 1650 nm. The strongest upconverted emission occurs at 0.1 mol%

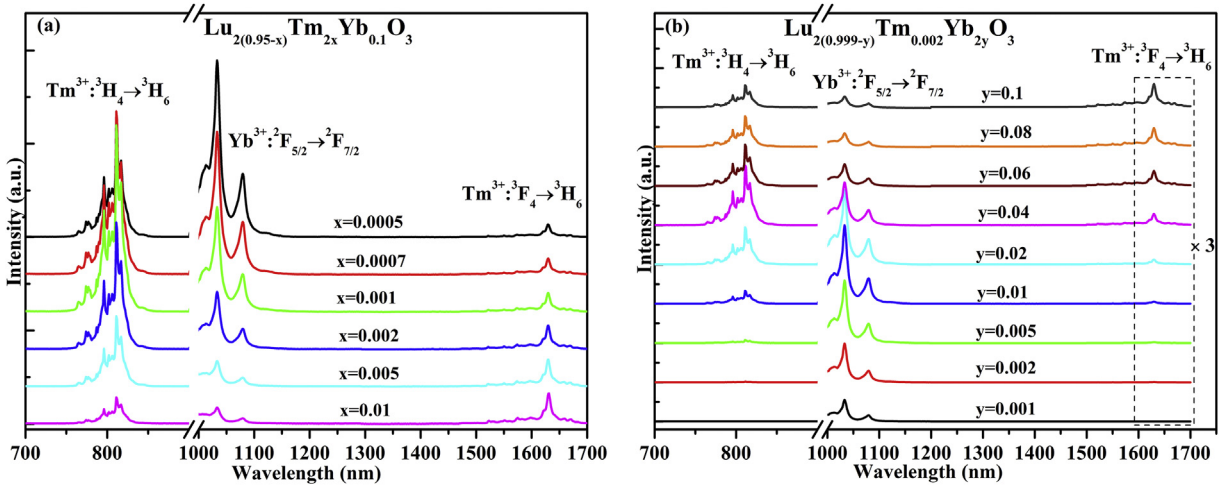

Fig. 2. Room temperature emission spectra of $Lu_{2(0.95-x)}Tm_{2x}Yb_{0.1}O_3$ ($x = 0.0005–0.01$) (a) and $Lu_{2(0.999-y)}Tm_{0.002}Yb_{2y}O_3$ ($y = 0.001–0.1$) (b) upon 980 nm excitation with a low pump density of 7 mW/mm^2.

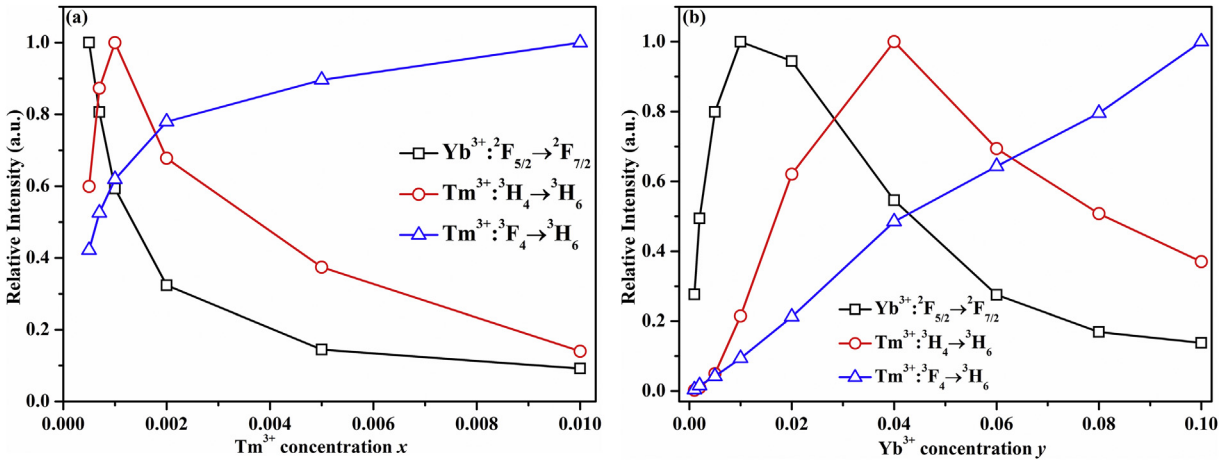

Fig. 3. Dependence of different emission intensities on Tm^{3+} doping concentration (a) and on Yb^{3+} doping concentration (b). The intensity of each transition is normalized by its maximum.

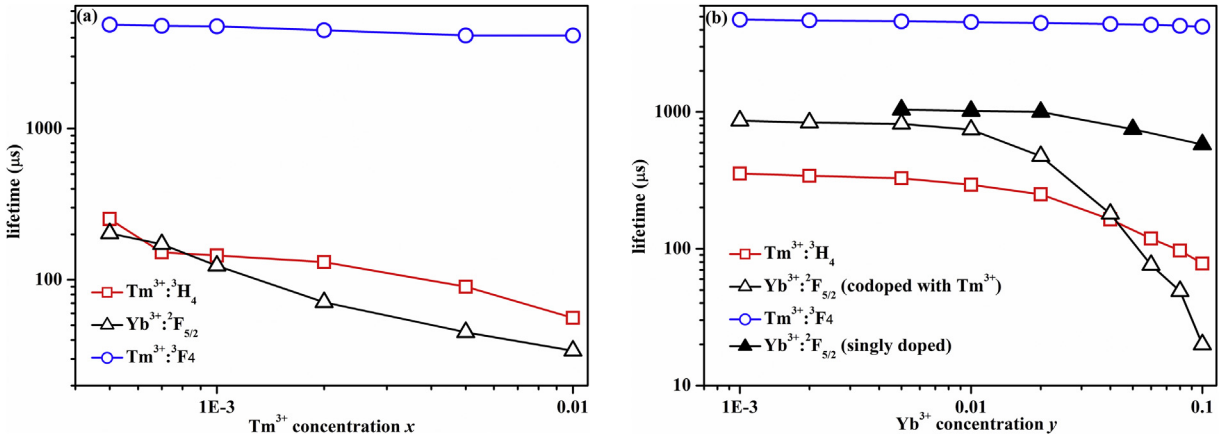

Fig. 4. Dependence of Yb^{3+}:$^2F_{5/2}$ and Tm^{3+}:$^3H_4$, $^3F_4$ levels lifetimes on Tm^{3+} concentration in $Lu_{2(0.95-x)}Tm_{2x}Yb_{0.1}O_3$ ($x = 0.0005–0.01$) (a) and on Yb^{3+} concentration in the sample series of $Lu_{2(0.999-y)}Tm_{0.002}Yb_{2y}O_3$ ($y = 0.001–0.1$) (b). The dependence of Yb^{3+}:$^2F_{5/2}$ lifetimes on Yb^{3+} concentration for the sample series of $Lu_{2(1-y)}Yb_{2y}O_3$ ($y = 0.005–0.1$) is also shown in (b).

Tm^{3+}. Accordingly, another sample series with a fixed Tm^{3+} concentration at 0.1 mol% and various Yb^{3+} concentrations ($y = 0.001–0.1$) are prepared and their emission spectra are shown in Fig. 2b. The strongest upconverted NIR emission is observed at 4 mol% Yb^{3+}. Fig. 3 shows the dependence of the emission intensities for Tm^{3+}: $^3H_4 \rightarrow {}^3H_6$, $^3F_4 \rightarrow {}^3H_6$ transitions, and Yb^{3+}: $^2F_{5/2} \rightarrow {}^2F_{7/2}$ transition on Tm^{3+} concentration and Yb^{3+} concentration. For the sample series of fixed 5 mol% Yb^{3+} concentration (Fig. 3a), one can find the enhancement of Tm^{3+}:$^3F_4 \rightarrow {}^3H_6$ emission on increasing Tm^{3+} concentration along with the decrease of Yb^{3+} emission, indicating the enhanced energy transfer due to the increased acceptor concentration. For the sample series of fixed 0.1 mol% Tm^{3+} concentration (Fig. 3b), it can be found that the intensity of Yb^{3+} emission increases with Yb^{3+} concentration and reaches the maximum at $y = 0.01$ and then decreases rapidly. Meanwhile, Tm^{3+}:$^3F_4 \rightarrow {}^3H_6$ emission always keeps growing up, meaning the enhanced energy transfer from Yb^{3+} to Tm^{3+}. In view of the fixed Tm^{3+} concentration, the enhancement of energy transfer can be attributed to the quickened excitation diffusion among Yb^{3+} ions.

One may wonder if the rapid decrease of the emission intensity of Yb^{3+} for $y > 0.01$ results from Yb^{3+} self-quenching [28,29]. However, we notice that the fluorescence lifetimes of Yb^{3+} are shortened much less for Yb^{3+} singly doping than for Yb^{3+} and 0.1 mol% Tm^{3+} codoping with the Yb^{3+} concentration higher than 0.01, as shown in Fig. 4b. This indicates that the rapid decrease of Yb^{3+} emission in the codoped samples is mainly due to enhanced energy transfer to Tm^{3+} rather than Yb^{3+} self-quenching.

Fig. 4a and b shows the dependence of lifetimes of Yb^{3+}:$^2F_{5/2}$ level and Tm^{3+}:$^3F_4$, $^3H_4$ levels on Tm^{3+} and Yb^{3+} concentrations in the sample series of $Lu_{2(0.95-x)}Tm_{2x}Yb_{0.1}O_3$ ($x = 0.0005–0.01$) and $Lu_{2(0.999-y)}Tm_{0.002}Yb_{2y}O_3$ ($y = 0–0.1$), respectively. The above lifetimes are summarized in Tables 1 and 2.

From Fig. 4, one can find that the lifetimes of Tm^{3+}:$^3F_4$ level are weakly dependent on the dopant concentration. In Fig. 4a the lifetimes of Tm^{3+}:$^3H_4$ level decrease with the increase of Tm^{3+} concentration, which is mainly caused by the cross relaxation process between Tm^{3+} ions, described as: (Tm^{3+}:$^3H_4$, Tm^{3+}:$^3H_6$) → (Tm^{3+}:$^3F_4$, Tm^{3+}:$^3F_4$) [30]. Meanwhile, the rapid shortening of the lifetime of Yb^{3+}:$^2F_{5/2}$ level with increasing Tm^{3+} concentration reflects the enhanced $Yb^{3+} \rightarrow Tm^{3+}$ energy transfer. The efficiency of energy transfer can be calculated by

$$\eta = 1 - \frac{\tau}{\tau_0} \quad (1)$$

where τ and τ_0 are the excited state lifetimes of donor in the

Table 1
The lifetimes and energy transfer efficiencies (η_{ET}) in $Lu_{2(0.95-x)}Tm_{2x}Yb_{0.1}O_3$ ($x = 0.0005–0.01$).

x	Tm^{3+}:$^3H_4$ (μs)	Yb^{3+}:$^2F_{5/2}$ (μs)	
	$\lambda_{EX} = 683$ nm	$\lambda_{EX} = 972$ nm	η_{ET} (%)
	$\lambda_{EM} = 811$ nm	$\lambda_{EM} = 1033$ nm	$\tau_0 = 750$ μs
0.0005	252	203	73
0.0007	152	172	77
0.001	145	124	83
0.002	131	71	91
0.005	90	45	94
0.01	56	34	95

Table 2
The lifetimes and energy back transfer efficiencies (η_{EBT}) in $Lu_{2(0.999-y)}Tm_{0.002}Yb_{2y}O_3$ ($y = 0.001–0.1$).

y	Tm^{3+}:$^3H_4$ (μs)	Tm^{3+}:$^3H_4$	Yb^{3+}:$^2F_{5/2}$(μs)
	$\lambda_{EX} = 683$ nm		$\lambda_{EX} = 972$ nm
	$\lambda_{EM} = 811$ nm	η_{EBT} (%)	$\lambda_{EM} = 1033$ nm
0	360		865
0.001	355	1	
0.002	342	5	838
0.005	328	9	820
0.01	294	18	744
0.02	250	31	476
0.04	164	54	180
0.06	119	67	76
0.08	97	73	49
0.1	78	78	20

presence and in the absence of acceptor, respectively. The calculated efficiencies of energy transfer from Yb^{3+} to Tm^{3+} using Eq. (1) are listed in Table 1. For the series of sample with a fixed 5 mol% Yb^{3+}, η_{ET} can reach 95% for Tm^{3+} concentration at $x = 0.01$.

In Fig. 4b, the decrease of the lifetimes of Tm^{3+}:$^3H_4$ level is observed with the increase of Yb^{3+} concentration, which is caused by the nonresonant energy back transfer from Tm^{3+} to Yb^{3+}, described as (Tm^{3+}:$^3H_4$, Yb^{3+}:$^2F_{7/2}$) → (Tm^{3+}:$^3H_6$, Yb^{3+}:$^2F_{5/2}$) [15,23]. The energy back transfer efficiency (η_{EBT}) can be calculated by Eq. (1) and the values are listed in Table 2. It is obvious that the efficiency η_{EBT} increases with increasing Yb^{3+} concentration, and reaches 78% when $y = 0.1$.

Fig. 5 shows the energy level diagram with two step energy transfers involved in the upconverted NIR emission of Tm^{3+} and Yb^{3+} codoped system. In the first step, Tm^{3+}:$^3H_5$ level is populated from the ground state $^3H_6$ and then relaxes down to the $^3F_4$ level. In the second step, the Tm^{3+}:$^3F_4$ level is further excited to the $^3F_{2,3}$ level, which rapidly relaxes down to the $^3H_4$ level. To understand the important influence of excitation diffusion on the energy transfer rates in the two step energy transfers, the dependence of the emission intensities on dopant concentration (see Fig. 3) is analyzed as follows.

In the first step energy transfer upon continuous 980 nm excitation, the state populations n_1 for Tm^{3+}:$^3F_4$ level, n_0 for the ground $^3H_6$ level of Tm^{3+} and n_d for Yb^{3+} $^2F_{5/2}$ level satisfy

$$\frac{n_1}{\tau_1} = (c_1 n_0 + k_1 n_0) n_d \quad (2)$$

where τ_1 is the lifetime of Tm^{3+}:$^3F_4$ level, c_1 is the coefficient for the first step energy transfer rate in the absence of excitation diffusion among Yb^{3+} ions, k_1 is the coefficient for the additional transfer rate in the presence of excitation diffusion among Yb^{3+} ions and it thus depends on Yb^{3+} concentration. The terms in the brackets are the

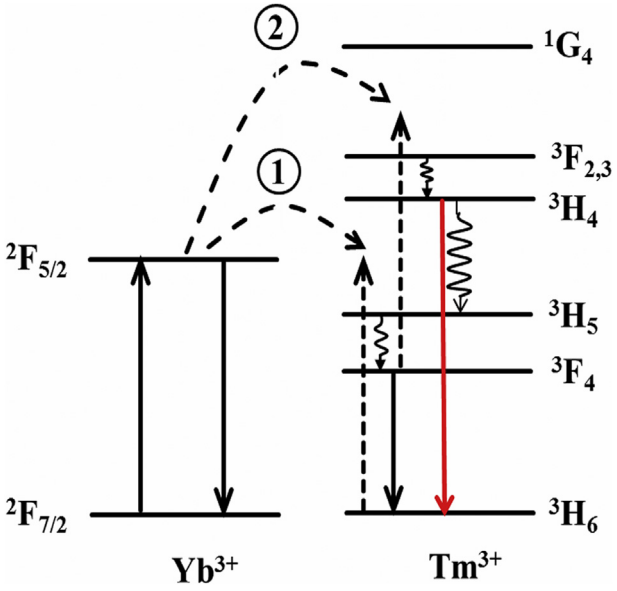

Fig. 5. Energy level diagrams and upconversion mechanisms in Tm^{3+} and Yb^{3+} codoped materials under 980 nm excitation.

total transfer rate. For weak excitation in the present wok, n_0 is close to the Tm^{3+} concentration x.

According to Eq. (2), the coefficient c_1+k_1 is thus proportional to $Tm^{3+}(^3F_4)/[Yb^{3+}(^2F_{5/2})x\tau_1]$, where $Tm^{3+}(^3F_4)$ and $Yb^{3+}(^2F_{5/2})$ are the intensities of Tm^{3+}:$^3F_4 \rightarrow {}^3H_6$ and Yb^{3+}:$^2F_{5/2} \rightarrow {}^2F_{7/2}$ emissions, respectively. Based on the data in Fig. 3, the variation of the ratio c_1+k_1 with Tm^{3+} and Yb^{3+} concentrations are obtained and plotted in Fig. 6a and b, respectively. It exhibits that c_1+k_1 increases little with the increase of Tm^{3+} concentration from 0.0005 to 0.01, but it increases quadratically by 500 times with increasing Yb^{3+} concentration from $y = 0.001$ to 0.1. The quadratic increase makes c_1+k_1 increase by 14.5 times for $y = 0.02$, 60 times for $y = 0.04$, and 160 times for $y = 0.06$, meaning $k_1 \gg c_1$ for $y > 0.02$. In the theory of energy transfer [22], k_1 is dependent on Yb^{3+} concentration but independent on Tm^{3+} concentration; c_1 is proportional to x for high Tm^{3+} concentration but independent on Yb^{3+} concentration. Therefore, the little increase of c_1+k_1 with increasing x for a fixed 5 mol% Yb^{3+} is due to $k_1 \gg c_1$. The quadratic increase indicates that k_1 is proportional to y^2. According to Dexter's theory for concentration quenching [22], the energy transfer rate is the product of y^2 and a coefficient which may be related to y. If the acceptor acts as a quencher that can completely quench the donor within a constant distance as described by Perrin model [31], the energy transfer rate is proportional to the product of y^2 and x, hence k_1 is proportional to y^2 from Eq. (2). The acceptors in Perrin model perhaps interact with donors by exchange mechanism.

In the second step energy transfer, we have

$$\frac{n_2}{\tau_2} = (c_2 n_1 + k_2 n_1 + l_2 n_1) n_d \quad (3)$$

where n_2 and τ_2 are the population and lifetime of Tm^{3+}: $^3H_4$ level, respectively, c_2 is the coefficient for the second step energy transfer rate in the absence of excitation diffusion among Yb^{3+} ions, k_2 is the coefficient for the additional transfer rate in the presence of excitation diffusion among Yb^{3+} ions, and l_2 is the coefficient for the additional transfer rate in the presence of excitation diffusion in the excited state of Tm^{3+}:$^3F_4$ level, depending on Tm^{3+} concentration. From Eq. (3) the ratio $n_2/(n_d\, n_1\tau_2)$ is proportional to $c_2+k_2+l_2$, of which the dependence on Tm^{3+} concentration and Yb^{3+}

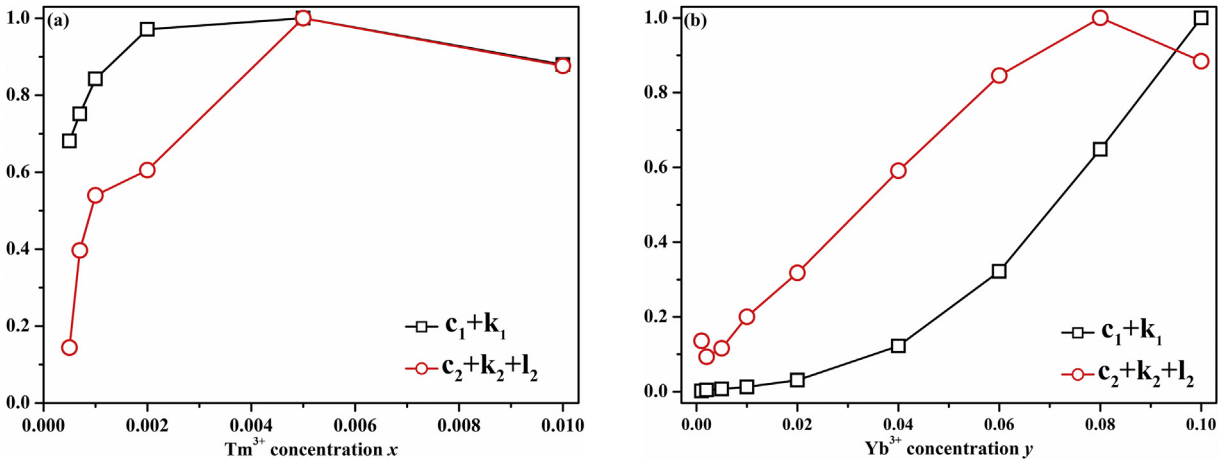

Fig. 6. Dependence of total coefficients c_1+k_1 and $c_2+k_2+l_2$ on Tm^{3+} concentration (a) and on Yb^{3+} concentration (b). The maximal value of each ratio is normalized.

concentration are obtained in terms of $Tm^{3+}(^3H_4)/[Tm^{3+}(^3F_4)$ $Yb^{3+}(^2F_{5/2})\tau_2]$ and plotted in Fig. 6a and b, respectively. One can find in Fig. 6a that $c_2+k_2+l_2$ increases with increasing x and it is saturated for $x > 0.005$. In view of the low population of Tm^{3+}:$^3F_4$ level under weak excitation condition in our case, c_2 is independent on n_1, k_2 is only dependent on Yb^{3+} concentration, and l_2 is dependent on Tm^{3+} concentration. Accordingly, the enhanced $c_2+k_2+l_2$ on increasing x is attributed to the increment of l_2 due to the excitation diffusion among excited Tm^{3+} in the $^3F_4$ level. The $c_2+k_2+l_2$ increases by 3.9 times with increasing x from 0.0005 to 0.001, and by 6.3 times for $x > 0.005$. The subsequent saturation can be explained as the reach of the transfer limit where the diffusion among donors is much more rapid than transfer to acceptors, which is easily achieved because the concentration of the acceptor, Tm^{3+}:$^3F_4$ is very low [32]. A similar increase trend of $c_2+k_2+l_2$ on increasing y is also observed, as shown in Fig. 6b. A linear increase appears on increasing y up to 0.08, and a saturation behavior is observed for $y > 0.08$, reflecting the feature of k_2 and the transfer limit. The $c_2+k_2+l_2$ increases by 6.6 times with increasing y from 0.001 to 0.04 and 11.1 times for $y > 0.08$. One may find that the value of c_1+k_1 increases by 500 times with increasing Yb^{3+} concentration from 0 to 0.1 while $c_2+k_2+l_2$ only increases by 11.1 times. It can be explained as follows. The concentration of Tm^{3+} is fixed at a low value 0.1 mol%, which will lead the population of the intermediate level of Tm^{3+}:$^3F_4$ much lower than 0.1 mol% under weak excitation condition. In this case, k_2 could be more easier to reach saturation than k_1, and it may have started at an even lower Yb^{3+} concentration (maybe at $y < 0.01$), if the population of Tm^{3+}:$^3F_4$ level is low enough. The linear relationship of k_2 with the donor concentration was expected by dexter based on dipole-dipole energy transfer between donors and between a donor and an accepter [22]. It is concluded that the excitation diffusions among Yb^{3+} ions and among Tm^{3+} ions substantially enhance the rate of energy transfer from Yb^{3+} to Tm^{3+} and thus dominate the energy transfer upconversion in Tm^{3+} and Yb^{3+} codoped Lu_2O_3 with the optimized concentrations of 0.1 mol% Tm^{3+} and 4 mol% Yb^{3+} for the strongest upconverted NIR emission.

4. Conclusions

The energy transfer upconversion process in Lu_2O_3:Tm^{3+}, Yb^{3+} in the infrared region are investigated in detail as a function of dopant concentration. From the dependence of the emissions intensities of Tm^{3+}:$^3F_4$, $^3H_4$ levels and Yb^{3+}:$^2F_{5/2}$ level on Tm^{3+} and/or Yb^{3+} concentration, the optimal doping concentration for the upconverted NIR emission around 811 nm is determined to be 0.1 mol% Tm^{3+} and 4 mol% Yb^{3+}. The energy transfer efficiency (η_{ET}) from Yb^{3+} to Tm^{3+} can reach up to 83% for the optimized doping concentration. Based on the steady state equations, it is concluded that the total coefficient of the first step energy transfer increases linearly with Tm^{3+} concentration and quadratically with Yb^{3+} concentration. Notably, it increases by 500 times when Yb^{3+} concentration increases from $y = 0.001$ to $y = 0.1$. Moreover, the total coefficient of the second step energy transfer increases with Tm^{3+} concentration and reaches the saturation at $x > 0.005$, while it increases with Yb^{3+} concentration and reaches the saturation at $y > 0.08$ due to the rapid transfer rate limit.

The results indicate that the excitation diffusions among Yb^{3+} ions and among Tm^{3+} ions substantially enhance the rate of energy transfer from Yb^{3+} to Tm^{3+} and thus dominate the energy transfer upconversion process. The optimized upconverted NIR emission around 811 nm may find its applications in various fields like bioimaging. Besides, the discussions in Lu_2O_3:Tm^{3+}, Yb^{3+} can provide additional theoretical understanding of the step energy transfer upconversion process.

Acknowledgements

This work was partially supported by the National Key Research and Development Program of China (Grant No. 2016YFB0701003, 2016YFB0400605), National Natural Science Foundation of China (Grant No. 61275055, 11274007, 51402284 and 11604330), Natural Science Foundation of Jilin Province (Grant No. 20140101169JC, 20150520022JH and 20160520171JH), and the prior sci-tech program of innovation and entrepreneurship of oversea Chinese talent of Jilin province.

References

[1] H.A. Höppe, Recent developments in the field of inorganic phosphors, Angew. Chem. Int. Ed. 48 (2009) 3572–3582.
[2] Q. Zhan, J. Qian, H. Liang, G. Somesfalean, D. Wang, S. He, Z. Zhang, S. Andersson-Engels, Using 915 nm laser excited $Tm^{3+}/Er^{3+}/Ho^{3+}$-doped $NaYbF_4$ upconversion nanoparticles for in vitro and deeper in vivo bioimaging without overheating irradiation, ACS Nano 5 (2011) 3744–3757.
[3] S. Schietinger, T. Aichele, H.Q. Wang, T. Nann, O. Benson, Plasmon-enhanced upconversion in single $NaYF_4$:Yb^{3+}/Er^{3+} codoped nanocrystals, Nano Lett. 10 (2009) 134–138.
[4] A.M. Smith, M.C. Mancini, S. Nie, Second window for in vivo imaging, Nat. Nanotechnol. 4 (2009) 710–711.
[5] J. Zhang, Z. Hao, J. Li, X. Zhang, Y. Luo, G. Pan, Observation of efficient population of the red-emitting state from the green state by non-multiphonon relaxation in the Er^{3+}–Yb^{3+} system, Light Sci. Appl. 4 (2015) e239.

[6] Y.J. Liang, F. Liu, Y.F. Chen, X.J. Wang, K.N. Sun, Z.W. Pan, New function of the Yb^{3+} ion as an efficient emitter of persistent luminescence in the short-wave infrared, Light Sci. Appl. 5 (2016) e16124.
[7] L. Zhang, S. Zhao, Z. Liang, J. Zhang, W. Zhu, P. Liu, H. Sun, The colour tuning of upconversion emission from green to red in $NaScF_4$:Yb^{3+}/Er^{3+} nanocrystals by adjusting the reaction time, J. Alloys Compd. 699 (2017) 1–6.
[8] H. Zhang, T. Jia, X. Shang, S. Zhang, Z. Sun, J. Qiu, Mechanisms of the blue emission of $NaYF_4$:Tm^{3+} nanoparticles excited by an 800 nm continuous wave laser, Phys. Chem. Chem. Phys. 18 (2016) 25905–25914.
[9] G. Jalani, R. Naccache, D.H. Rosenzweig, S. Lerouge, L. Haglund, F. Vetrone, M. Cerruti, Real-time, non-invasive monitoring of hydrogel degradation using $LiYF_4$:Yb^{3+}/Tm^{3+} NIR-to-NIR upconverting nanoparticles, Nanoscale 7 (2015) 11255–11262.
[10] M. Nyk, R. Kumar, T.Y. Ohulchanskyy, E.J. Bergey, P.N. Prasad, High contrast in vitro and in vivo photoluminescence bioimaging using near infrared to near infrared up-conversion in Tm^{3+} and Yb^{3+} doped fluoride nanophosphors, Nano Lett. 8 (2008) 3834–3838.
[11] V. Mahalingam, F. Vetrone, R. Naccache, A. Speghini, J.A. Capobianco, Colloidal Tm^{3+}/Yb^{3+}-doped $LiYF_4$ nanocrystals: multiple luminescence spanning the UV to NIR regions via low-energy excitation, Adv. Mater. 21 (2009) 4025–4028.
[12] L. Liu, F. Qin, H. Zhao, T. Lv, Z. Zhang, W. Cao, Facile synthesis and upconversion luminescence of β-$NaYF_4$:Yb, Tm nanocrystals with highly tunable and uniform β-$NaYF_4$ shells, J. Alloys Compd. 684 (2016) 211–216.
[13] Y. Huang, S. Sun, F. Yuan, L. Zhang, Z. Lin, Spectroscopic properties and continuous-wave laser operation of Er^{3+}:Yb^{3+}:$LaMgB_5O_{10}$ crystal, J. Alloys Compd. 695 (2017) 215–220.
[14] W.P. Qin, Z.Y. Liu, C.N. Sin, C.F. Wu, G.S. Qin, Z. Chen, K.Z. Zheng, Multi-ion cooperative processes in Yb^{3+} clusters, Light Sci. Appl. 3 (2014) e193.
[15] F.W. Ostermayer Jr., J.P. Van der Ziel, H.M. Marcos, L.G. Van Uitert, J.E. Geusic, Frequency upconversion in YF_3: Yb^{3+},Tm^{3+}, Phys. Rev. B 3 (1971) 2698.
[16] Y. Mita, M. Togashi, Y. Umetsu, H. Yamamoto, Energy transfer processes in Yb^{3+}-and Tm^{3+}-ion-doped oxide and fluoride crystals, Jpn. J. Appl. Phys. 40 (2001) 5925.
[17] I. Etchart, I. Hernández, A. Huignard, M. Bérard, M. Laroche, W.P. Gillin, R.J. Curry, A.K. Cheetham, Oxide phosphors for light upconversion; Yb^{3+} and Tm^{3+} co-doped Y_2BaZnO_5, J. Appl. Phys. 109 (2011) 063104.
[18] V. Mahalingam, F. Mangiarini, F. Vetrone, V. Venkatramu, M. Bettinelli, A. Speghini, J.A. Capobianco, Bright white upconversion emission from Tm^{3+}/Yb^{3+}/Er^{3+}-doped $Lu_3Ga_5O_{12}$ nanocrystals, J. Phys. Chem. C 112 (2008) 17745–17749.
[19] X. Hou, S. Zhou, H. Lin, H. Teng, Y. Li, W. Li, T. Jia, Violet and blue upconversion luminescence in Tm^{3+}/Yb^{3+} codoped Y_2O_3 transparent ceramic, J. Appl. Phys. 107 (2010) 83101.
[20] L. Li, H. Lin, X. Zhao, Y. Wang, X. Zhou, C. Ma, X. Wei, Effect of Yb^{3+} concentration on upconversion luminescence in Yb^{3+}, Tm^{3+} co-doped Lu_2O_3 nanophosphors, J. Alloys Compd. 586 (2014) 555–560.
[21] J. Yang, C. Zhang, C. Peng, C. Li, L. Wang, R. Chai, J. Lin, Controllable Red, Green, Blue (RGB) and bright white upconversion luminescence of Lu_2O_3:Yb^{3+}/Er^{3+}/Tm^{3+} nanocrystals through single laser excitation at 980 nm, Chem Eur. J. 15 (2009) 4649–4655.
[22] D.L. Dexter, J.H. Schulman, Theory of concentration quenching in inorganic phosphors, J. Chem. Phys. 22 (1954) 1063–1070.
[23] J. Li, J. Zhang, Z. Hao, X. Zhang, J. Zhao, Y. Luo, Upconversion properties and dynamics study in Tm^{3+} and Yb^{3+} codoped $CaSc_2O_4$ oxide material, J. Appl. Phys. 113 (2013) 223507.
[24] L. Huang, S. Shen, A. Jha, Near infrared spectroscopic investigation of Tm^{3+}–Yb^{3+} co-doped tellurite glasses, J. Non Cryst. Solids 345 (2004) 349–353.
[25] F. Pandozzi, F. Vetrone, J.C. Boyer, R. Naccache, J.A. Capobianco, A. Speghini, M. Bettinelli, A spectroscopic analysis of blue and ultraviolet upconverted emissions from $Gd_3Ga_5O_{12}$:Tm^{3+}, Yb^{3+} nanocrystals, J. Phys. Chem. B 109 (2005) 17400–17405.
[26] D.A. Simpson, W.E. Gibbs, S.F. Collins, W. Blanc, B. Dussardier, G. Monnom, P. Peterka, G.W. Baxter, Visible and near infra-red up-conversion in Tm^{3+}/Yb^{3+} co-doped silica fibers under 980 nm excitation, Opt. Express 16 (2008) 13781–13799.
[27] Z. Feng, H. Xia, C. Wang, Z. Zhang, D. Jiang, J. Zhang, Q. Sheng, X. Gu, Y. Zhang, B. Chen, H. Jiang, 1.8 μm luminescent properties and energy transfer of Yb^{3+}/Tm^{3+} co-doped α-$NaYF_4$ single crystals, J. Alloys Compd. 680 (2016) 26–30.
[28] Y. Guyot, H. Canibano, C. Goutaudier, A. Novoselov, A. Yoshikawa, T. Fukuda, G. Boulon, Yb^{3+}-doped $Gd_3Ga_5O_{12}$ garnet single crystals grown by the micro-pulling down technique for laser application. Part 2: concentration quenching analysis and laser optimization, Opt. Mater. 28 (2006) 1–8.
[29] F. Auzel, G. Baldacchini, L. Laversenne, G. Boulon, Radiation trapping and self-quenching analysis in Yb^{3+}, Er^{3+}, and Ho^{3+} doped Y_2O_3, Opt. Mater. 24 (2003) 103–109.
[30] D.C. Yu, R. Martín-Rodríguez, Q.Y. Zhang, A. Meijerink, F.T. Rabouw, Multi-photon quantum cutting in Gd_2O_2S: Tm^{3+} to enhance the photo-response of solar cells, Light Sci. Appl. 4 (2015) e344.
[31] M. Inokuti, F. Hirayama, Influence of energy transfer by the exchange mechanism on donor luminescence, J. Chem. Phys. 43 (1965) 1978–1989.
[32] Y. Mita, H. Kawashima, N. Sawanobori, Energy transfer characteristics in Yb^{3+}-and Tm^{3+}-doped fluoride glass, Jpn. J. Appl. Phys. 38 (1999) 746.